International Journal of Geographical Information Science, 2015
Vol. 29, No. 12, 2041–2060, http://dx.doi.org/10.1080/13658816.2015.1038719

Taylor & Francis
Taylor & Francis Group

A localized contour tree method for deriving geometric and topological properties of complex surface depressions based on high-resolution topographical data

Qiusheng Wu[a], Hongxing Liu[a]*, Shujie Wang[a], Bailang Yu[b], Richard Beck[a] and Kenneth Hinkel[a]

[a]*Department of Geography, University of Cincinnati, Cincinnati, OH, USA;* [b]*Key Laboratory of Geographic Information Science, Ministry of Education, East China Normal University, Shanghai, China*

(*Received 3 December 2014; final version received 11 March 2015*)

Surface depressions are abundant in topographically complex landscapes, and they exert significant influences on hydrological, ecological, and biogeochemical processes at local and regional scales. The increasing availability of high-resolution topographical data makes it possible to resolve small surface depressions. By analogy with the reasoning process of a human interpreter to visually recognize surface depressions from a topographic map, we developed a localized contour tree method that is able to fully exploit high-resolution topographical data for detecting, delineating, and characterizing surface depressions across scales with a multitude of geometric and topological properties. In this research, we introduce a new concept 'pour contour' and a graph theory-based contour tree representation for the first time to tackle the surface depression detection and delineation problem. Beyond the depression detection and filling addressed in the previous raster-based methods, our localized contour tree method derives the location, perimeter, surface area, depth, spill elevation, storage volume, shape index, and other geometric properties for all individual surface depressions, as well as the nested topological structures for complex surface depressions. The combination of various geometric properties and nested topological descriptions provides comprehensive and essential information about surface depressions across scales for various environmental applications, such as fine-scale ecohydrological modeling, limnological analyses, and wetland studies. Our application example demonstrated that our localized contour tree method is functionally effective and computationally efficient.

Keywords: depressions; contour tree; pour contour; topology; geometric properties; LiDAR

1. Introduction

A depression is a sunken area on Earth's surface surrounded by higher ground in all directions. Surface depressions are bowl-like landforms across a range of spatial scales. They are formed by either natural or anthropogenic processes. Natural surface depressions are abundant in topographically complex landscapes, particularly in glaciated, karst, volcanic, or Aeolian landscapes (e.g., Mark 1988, Martz and Jong 1988, Muehrcke *et al.* 1992, Tribe 1992, Macmillan *et al.* 1993, Huang *et al.* 2014). Examples of natural depressions include glaciated kettle lakes, cirques, prairie potholes, karst sinkholes,

*Corresponding author. Email: Hongxing.Liu@uc.edu

volcanic craters, pit craters, impact craters, etc. Some surface depressions are related to a variety of human activities, such as constructing detention basins and reservoirs, mining, quarrying, charcoal or lime production, or bombing.

Surface depressions trap, collect, and often hold overland runoff from higher areas of their closed interior drainage basins during rainfall events and snowmelt in the spring. Therefore, they are often covered by water temporarily, seasonally or permanently, forming wetlands, ponds, or lakes landscapes. Depressions trap and store sediment and nutrients, enhance water loss to the atmosphere via evaporation and to groundwater via infiltration, and provide critical habitats for plants and animals (Hubbard and Linder 1986, Rosenberry and Winter 1997, Hayashi and Van Der Kamp 2000, Antonić *et al.* 2001), having profound impacts on local or regional hydrological, ecological, and biogeochemical processes. The existence and density of surface depressions control hydrological partitioning of rainfall into infiltration and runoff (Dunne *et al.* 1991, Frei *et al.* 2010, Thompson *et al.* 2010, Loos and Elsenbeer 2011) and hydrological connectivity (Li *et al.* 2011), influence soil moisture states (Simmons *et al.* 2011) and vegetation patterns (Moser *et al.* 2007, Scanlon *et al.* 2007, Mcgrath *et al.* 2012), regulate runoff water quality through trapping and filtering pollutants, wastes, sediments, and excess nutrients (Wörman and Kronnäs 2005), and create the wet and nutrient-rich environmental conditions for many species to exist and reproduce (Antonić *et al.* 2001). The vital hydrological and ecological effects of surface depressions are largely determined by their geographical location, surface area, depth, storage volume, geometric shape, and other properties (Guo 1999, Wörman and Kronnäs 2005). Some of these properties are changing over time due to sedimentation, erosion, vegetation dynamics, and other processes. Detection, delineation, and quantitative characterization of surface depressions with accurate and up-to-date information are critical to many scientific studies and practical applications, such as ecohydrological modeling, limnological analyses, and wetland conservation and management.

However, most previous studies were based on coarse-resolution topographical data, in which surface depressions are treated as nuisance or spurious features (Jenson and Domingue 1988). This is because coarse-resolution topographic data are unable to reliably resolve small surface depressions and the noise and error in the topographic data tend to create artifact depressions, which are difficult to be distinguished from real surface depression features (Lindsay and Creed 2006). In a standard hydrological analysis, surface depressions are identified and then simply removed to create a depressionless surface topography, which ensure that water flows continuously across the topographic surface to the watershed outlets (Maidment 2002) and that the derived stream networks are fully connected for runoff routing. Depressions are typically removed by raising the elevations in depressions with the depression-filling algorithm (O'callaghan and Mark 1984, Jenson and Domingue 1988, Planchon and Darboux 2002), or less commonly by lowering the elevations of the depression boundary with depression-breaching algorithm (Martz and Garbrecht 1999, Lindsay and Creed 2005). In the previous studies, little attention has been paid to the geometric and topological properties of surface depressions, and the effects of surface depressions on local and regional hydrology and ecology were largely ignored.

In recent decades, the advent of airborne light detection and ranging (LiDAR) and interferometric synthetic aperture radar (InSAR) remote sensing technologies have produced large volumes of highly accurate and densely sampled topographical measurements (1–5 m spatial resolution) (White and Wang 2003, Finkl *et al.* 2005). The increasing availability of high-resolution topographical data allows for an entirely new level of detailed delineation and analyses of small-scale geomorphological features and landscape

structures at fine scales (Lefsky *et al.* 2002, Schwarz 2010, Ussyshkin and Theriault 2011). To fully exploit high-resolution topographical data for scientific investigation of hydrological and ecological effects of surface depressions, new algorithms and methods are required to efficiently delineate and quantify surface depressions across scales.

In this study, we present a new localized contour tree method for identifying and delineating surface depressions across scales and characterize their geometric properties and topological relationships. Our method is developed based on a novel concept of pour contour. The numerical algorithm for surface depression identification in our method is analogous to human visual interpretation of topographical contour maps. Based on the vector representation of surface topography as contours (Figure 1), we first establish the topological relationships between adjacent contours and then construct a contour tree based on the graph theory. By using a localized fast priority search algorithm over the contour tree, the pour contours are identified to represent surface depressions at different scales (levels). Surface area, storage volume, and other geometric properties are computed for each individual depression, and the nested topological relationships between surface depressions are also derived. The derived geometric properties and the nested hierarchical structure of surface depressions across scales would provide critical information for characterizing hydrological connectivity, simulating the dynamic filling–spilling–merging hydrological process, and examining the ecological and biogeochemical function of surface depressions on both natural and human-modified landscapes. Our application example demonstrates that our localized contour tree method is effective and efficient.

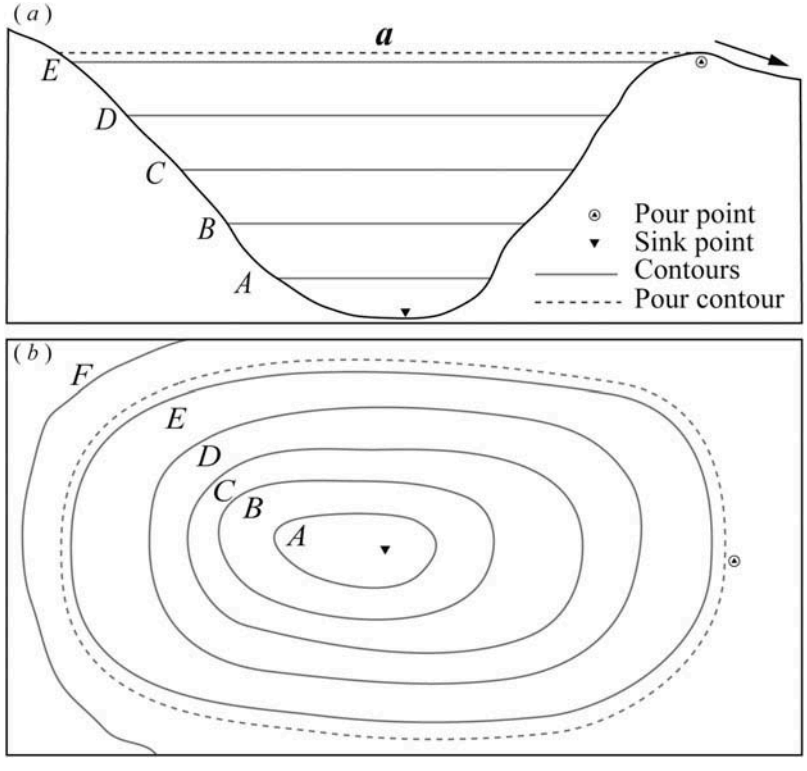

Figure 1. A simple surface depression: (a) longitudinal profile; (b) contour representation.

2. Numerical representation and geometric structure of surface depressions

Surface topography can be digitally represented by raster-based elevation grids digital elevation models (DEMs) or by vector-based equal elevation contour lines. In a DEM, a surface depression consists of a local minima and a set of spatially connected grid cells of low elevation, which are completely surrounded by embankment cells of higher elevation. The local minima at the depression bottom is referred to as a sink point or a pit (Figure 1), and its elevation is less than or equal to that of its eight neighbors. The sink point does not have a natural downslope flow path to watershed outlets, and the surrounding overland flow drains toward the sink point of the depression, forming an interior basin. When more runoff water drains to the depression, the water surface in it will eventually be raised to a certain level at which flood water starts to overflow from its perimeter. The lowest cell on the depression perimeter is referred to as the pour point, where water would pour out if the depression is filled up with water. Geometrically, the boundary of a surface depression is defined by the maximum level water surface, when flood water fills up the depression and starts to spill out (Figure 1). The elevation of the depression pour point is referred to as spill elevation (Wang and Liu 2006). The boundary of a surface depression indicates the spatial extent of the pond/lake created by flooding the depression.

In vector-based contour representation, a surface depression is indicated by a series of concentric closed contours with the inner contours having lower elevation than their outer surrounding (Figure 1). Similarly, a hill has a concentric pattern of closed contours, but the elevation value increases from outer contours to inner contours. On a topographical map, small tick marks or hachures, special cartographic symbols, are applied to the closed contour lines of the depression, with hachures pointing downslope. Such contours are referred to as hachured contour lines or depression contour lines. The sink point is located inside the innermost closed contour line. The outermost closed contour line of the depression indicates the spatial extent (boundary) of the depression. The elevation of the outermost closed contour approximates the spill elevation.

Surface depressions may vary in size, depth, and shape. The composition and structure of surface depressions can be highly complex (Hayashi *et al.* 2003). Some surface depressions might contain flat areas and other smaller nested depressions. On a topographical contour map, the complex surface depressions are manifested by the nested relationships of several sets of concentric closed contours (Figure 2). The nested hierarchical structure of surface depressions controls the dynamic filling–spilling–merging hydrological process.

Surface depressions detected from a DEM or a contour map could be real landscape features or spurious artifacts. Artifact depressions are not actual bowl-like landforms. They are caused by topographical data noise and errors, such as original measurement errors, data truncation or rounding errors, interpolation defects during data processing, and the limited horizontal and vertical resolution of DEMs (Tribe 1992, Martz and Garbrecht 1999). Artifact depressions are very common in coarse-resolution DEMs, particularly for the low-relief terrain (Tarboton *et al.* 1991, Tribe 1992, Martz and Garbrecht 1999). Despite superior spatial resolution and high vertical accuracy, high-resolution DEMs from LiDAR and InSAR technologies may also contain depression artifacts due to their imperfections (Arnold 2010, Lindsay and Creed 2006, Wang and Liu 2006, Li *et al.* 2011). Artifact depressions are often characterized by small size, shallowness, or irregular shapes (Wang and Liu 2006).

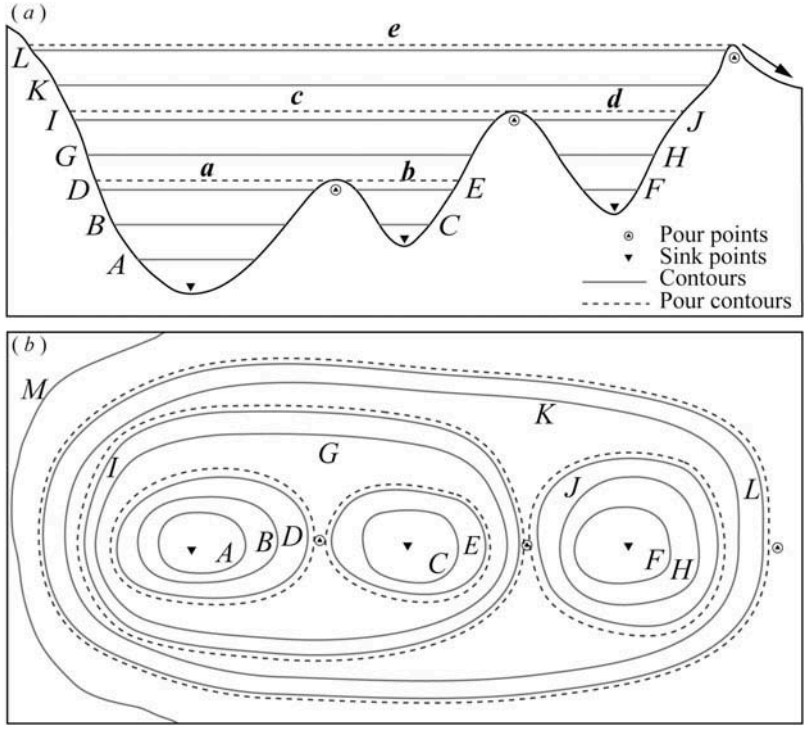

Figure 2. A composite surface depression with nested hierarchical structure: (a) longitudinal profile; (b) contour representation.

3. A localized contour tree method

3.1. *Previous algorithms and overview of our method*

A number of algorithms and methods have been proposed to treat surface depressions in the literature (Marks *et al.* 1984, Jenson and Domingue 1988, Planchon and Darboux 2002, Lindsay and Creed 2006, Wang and Liu 2006, Barnes *et al.* 2014) . The most widely used conventional method for handling surface depressions was developed by Jenson and Domingue (1988). This conventional method is overly time-consuming and deficient for handling large high-resolution DEM data sets. To process massive LiDAR DEMs for surface depression delineation, Wang and Liu (2006) developed a very efficient algorithm to identify and fill surface depressions by introducing the concept of spill elevation and integrating the priority queue data structure into the least-cost search of spill paths. Due to its high computation efficiency and coding simplicity and compactness, the priority-flood algorithm of Wang and Liu (2006) has been widely adopted and implemented by several open-source GIS software packages, e.g., SAGA GIS (http://www.saga-gis.org/) and Whitebox Geospatial Analysis Tools (GAT) (http://www.uoguelph.ca/~hydrogeo/Whitebox/). A number of variants of the priority-flood algorithm with a varying time complexity have been proposed (Jenson and Domingue 1988, Planchon and Darboux 2002, Wang and Liu 2006, Barnes *et al.* 2014, Yu *et al.* 2014), and a detailed review is provided by Barnes *et al.* (2014). To distinguish real surface depressions from artifacts, Lindsay and Creed (2006) developed a stochastic depression analysis method. In their method, the Monte Carlo procedure is utilized to create a random

error grid, which is then filled by using the priority-flood algorithm of Wang and Liu (2006). The probability of a depression occurring at any given location is calculated as the ratio of the number of depression occurrences to the total number of iterations. Those with a probability higher than a user-specified threshold value are identified as real surface depressions. The stochastic depression analysis algorithm of Lindsay and Creed (2006) has been implemented as a plug-in tool in Whitebox GAT, a powerful open-source GIS and remote sensing software package (Lindsay 2005, 2014, Lindsay and Seibert 2013) developed at the University of Guelph's Centre for Hydrogeomatics.

Previous studies have focused on identifying and filling surface depressions based on raster-based DEMs for hydrological modeling of overland flow (surface runoff) (Lindsay 2004, Wu *et al.* 2014). So far, little research has been directed to the quantitative characterization of surface depressions or the explicit representation and derivation of spatial relationships between surface depressions, although the newly emerged high-resolution topographical data contains sufficient information to reliably resolve even small-scale surface depression features. To fill up this research gap, we developed a localized contour tree method.

In contrast to previous studies, our method is based on the vector-based contour representation of surface topography. The computational algorithm of our method is conceptually similar to the reasoning logic of human visual interpretation of surface depressions on a topographical map, namely identifying surface depressions through finding sets of concentric closed contours with the decreasing elevation toward the inner center. It includes four key technical components: (1) identify the 'seed contours' to construct local contour trees to represent the topological relationships between adjacent closed contours based on the graph theory; (2) identify quasi 'pour contours' to approximate surface depressions by fast breadth-first priority search (Sedgewick 1998) over each local contour tree; (3) use an outer expansion algorithm to determine true 'pour contours' to precisely delineate surface depressions and then compute their geometric and volumetric properties; and (4) simplify local contour trees by removing non-pour contour nodes to derive explicit nested relationships between surface depressions across scales.

3.2. Identification of seed contours and construction of local contour trees

Contour lines can be derived from a DEM consisting of regularly distributed elevation points or from the Triangulated Irregular Networks (TINs) consists of irregularly distributed elevation points. The position and density of contour lines are determined by two important parameters: the base contour line and the contour interval. The data noise or errors in the DEM or TIN may lead to jagged, irregular, or fragmented contour lines. The common practice to reduce data noise is to smooth the DEM by a filtering operation prior to generating contours. A Gaussian or median filter can be used to remove data noise and suppress small artifact depressions without distorting the boundaries of true topographical depressions (Liu *et al.* 2010). Contours are then created based on the smoothed DEM with an appropriate contour interval.

There are two types of contours: closed contours and open contours. An open contour has a starting and an ending point that intersect map edges at different locations (e.g., contour ***F*** in Figure 1), while a closed contour is continuous without intersections with the map edges, forming a loop (e.g., contours ***A, B, C, D***, and ***E*** in Figure 1) (Lindsay 2004). To detect surface depressions, we only need to examine closed contours with a concentric pattern, while all open contours are ignored in the subsequent analysis. First, we identify 'seed contours' to construct local contour trees. A seed contour is a closed contour that

contains a sink point, but does not contain any other contours inside. The seed contour is the innermost closed contour, which may be surrounded by other contours. As shown in Figure 2, contours ***A***, ***C***, and ***F*** are seed contours, whereas contours ***B***, ***D***, ***E***, ***G***, ***H***, ***I***, ***J***, ***K***, and ***L*** are not. We prioritize the local contour tree construction in terms of the elevation value of the identified seed contours, and the seed contour with the lowest elevation value is first processed in the queue.

The contour tree is a conceptual data structure for describing the relationships among contours (Kweon and Kanade 1994). A contour map can be transferred into a graph with a tree structure (Boyell and Ruston 1963). In the present work, we use the contour tree to represent the topological relationship between adjacent contours within a set of concentric closed contours. The tree is composed of a root node, a set of internal nodes (branches), and a set of terminal nodes (leaves). The nodes in the tree represent closed contours, and the link (edge) between nodes represents the containment relationship between two adjacent closed contours. Each node in a contour tree has only one parent node, but may have one or more child nodes. If an internal node has two or more child nodes, it is called fork (or join) node. The two or more child nodes of a fork node are called split nodes. We construct the contour tree in a bottom-up manner with a tree growing algorithm. For a simple surface depression shown in Figure 1, the contour tree is initiated with the seed contour ***A*** as the leaf (terminal) node, which is the first-level contour at the bottom of the tree. Then, the contour tree is grown by searching and adding the adjacent closed contour ***B*** that contains the seed contour (leaf node) as its parent node. This iterative process continues, until the surrounding outermost closed contour ***E*** is included as the root node. The single-level surface depression leads to a simple one-branch contour tree (Figure 3a).

For a complex nested surface depression shown in Figure 2, the bottom-up tree growing algorithm results in a multibranch contour tree. The root node (***L*** in Figure 3b) has the highest elevation and directly or indirectly encloses all of the other closed

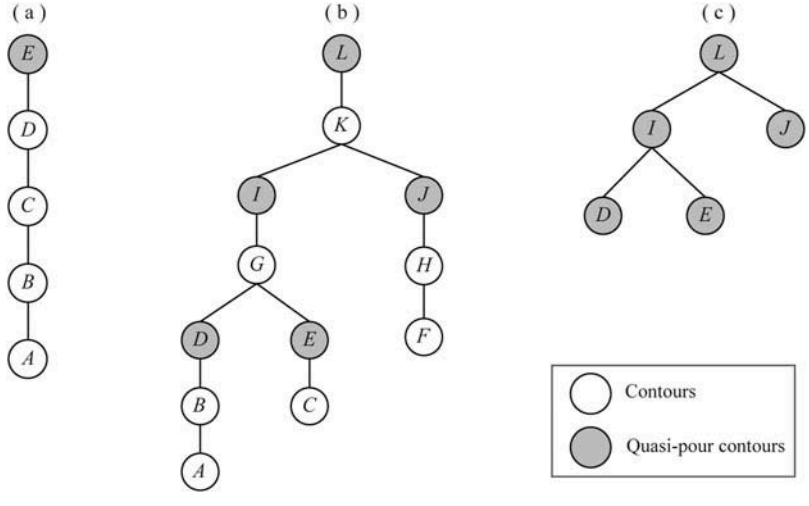

Figure 3. Illustration of local contour tree representation for surface depressions: (a) single-branch contour tree of the simple surface depression shown in Figure 1; (b) multibranch contour tree of the composite surface depression shown in Figure 2; (c) depression tree (simplified contour tree) of the composite surface depression shown in Figure 2.

contours. ***A***, ***C***, and ***F*** are the leaf nodes (seed contours) without child nodes. The split and merge at an internal node indicate the change in topological relationship. The fork node ***G*** has two child nodes (contours) of the same elevation, ***D*** and ***E.*** The contour tree embodies the dynamic filling–spilling–merging hydrological process of the nested hierarchical structure of depressions (Chu *et al.* 2013). When the overland runoff flows into the depression ***a*** and depression ***b*** (Figure 2), its water surface would gradually increase from the leaf node level (seed contour) to the parent node level of higher elevation. When the water surfaces of depression ***a*** and depression ***b*** reach to their spill elevation ***SE1*** (Wang and Liu 2006), these two adjacent depressions would merge to form a larger complex depression ***c***, which is reflected by sibling nodes ***D*** and ***E*** join at fork node ***G*** in the contour tree (see Figure 3). When the water surface levels of depression ***c*** and depression ***d*** increase to above their spill elevation ***SE2***, these two depressions further combine to form an even more complex and larger surface depression ***e***, which corresponds to the merge of nodes ***I*** and ***J*** at node ***K***. Clearly, the contour tree contains the information about the nested hierarchical relationships between surface depressions of different scales. Each local contour tree represents one disjointed depression (simple or composite), and the number of trees in the forest represents the total number of disjointed depressions (single or composite) for the entire area.

3.3. Identification of quasi-pour contours through a priority breadth-first search spanning local contour trees

In this study, a surface depression is treated as a 2D spatial object whose spatial extent is defined by the maximum level water surface area when flood water completely fills up the depression and starts to spill out from its pour point. The boundary of a surface depression corresponds to a closed contour with the same elevation as its pour point, which is referred to as the pour contour in this study. The pour point of the depression is located on its pour contour. Therefore, the task of surface depression detection becomes the identification of pour contours. For a simple one-branch contour tree in Figure 3a, the root node ***E*** indicates the outermost closed contour of the single-level depression, which is surrounded by either open contours or closed contours with a lower elevation. The closed contour corresponding to the root node ***E*** is referred to as a quasi-pour contour. Due to the contour interval, the elevation value of the quasi-pour contour may be equal to or slightly smaller than the spill elevation, and the quasi-pour contour would be overlapped or contained by the true pour contour in a close vicinity (Figure 1). For a multibranch contour tree (Figure 3b), the root node ***L*** is a quasi-pour contour too, which approximates the boundary of the highest level surface depression ***e*** (Figure 2). The nodes ***I*** and ***J***, two child split nodes of the fork node ***K***, are two quasi-pour contours, approximately representing the boundaries of two surface depressions ***c*** and ***d*** (Figure 2). Similarly, the nodes ***D*** and ***E*** are the child nodes of the fork node ***G***. They are quasi-pour contours, approximately defining the boundaries of surface depressions ***a*** and ***b*** (Figure 2).

In a contour tree, the root node and the child split nodes of all fork nodes are quasi-contours, which approximates all surface depressions across scales. A breadth-first priority search algorithm is applied to the contour tree to find and label all quasi-pour contours, which recursively traverses the nodes in the order of left node, right node, and the parent node. The root node is always the last node to visit. More information about the breadth-first priority search algorithm can be found in Sedgewick (1998).

3.4. Determination of true pour contours and geometric properties of surface depressions

The elevation value of a quasi-pour contour may be equal to or lower than the spill elevation. The elevation difference between a quasi-pour contour and the true pour contour is always smaller than the contour interval. When the contour interval is sufficiently small, all quasi-contours would be very close to their true pour contour.

When a quasi-pour contour has a slightly smaller value than the spill elevation, the surface area and depth of the spatial object bounded by the quasi-pour contour would be accordingly smaller than those of the true pour contour. To get accurate measurements on the geometric properties of surface depressions, each quasi-pour contour is expanded outward within the contour interval to determine its true pour contour using an incremental buffering algorithm. The true pour contours are then used to define the boundaries of all surface depressions.

Using the true pour contours as the boundaries, we derived three sets of geometric properties for each surface depression: (1) planimetric attributes, (2) depth and volumetric attributes, and (3) shape attributes. Planimetric attributes include the geographical location of centroid point, perimeter, and surface area. Depth and volumetric attributes include mean depth, maximum depth, and storage volume of water detention capacity. Shape attributes include compact index, circularity, and asymmetry. The planimetric and shape attributes are calculated by treating the true pour contour as a polygon. The depth and volumetric attributes are calculated by statistical analysis of all elevation cells within the true pour polygon. The maximum depth of a surface depression is the elevation difference between pour point (spill elevation) and the sink point.

3.5. Derivation of explicit nested topological relationships of surface depressions through simplification of local contour trees

To explicitly represent the nested hierarchical structure of a complex surface depression, the local contour tree is simplified by removing the nodes that do not correspond to pour contours. The root node of the contour tree is kept in the simplification since it always represents a pour contour. By searching the contour tree top-down, we examine each node if it is a child split node of a fork node. We only keep the child split nodes of fork nodes and delete other nodes in the contour tree simplification.

After the simplification, the single branch contour tree only has the root node left (e.g., Figure 3a). The multibranch contour tree shown in Figure 3b is reduced to a smaller compact tree with only five nodes (Figure 3c). The simplified tree is referred to as the depression tree since all nodes are pour contours and represent surface depressions at different levels within a complex depression. The leaf nodes of the simplified depression tree represent simple depressions at the first level. The parent fork node of two leaf nodes in the depression tree represents a composite at the second level. The merging of a second-level depression node with other second-level depression nodes or with other first-level depression nodes forms a more complex third-level depression. The complexity level of a composite depression can be measured by the height of the depression tree, namely the length of the longest path from the root node to the leaf nodes. Traversing the depression tree top-down simulates the splitting of a large composite surface depression into smaller lower level depressions when water level decreases, while traversing the depression tree bottom-up emulates the merging of smaller lower level depressions into larger and more complex depressions when water level increases. A complex depression

may have more than one first-level simple depressions embedded within it. Figure 2 describes a complex depression ***e*** with three levels, in which three first-level depressions (***a, b, d***) and one second-level depression (***c***) are nested inside. The combination of the topological information about the nested hierarchical structure and the geometric attributes provides a comprehensive description and quantification of each individual surface depression across scales.

3.6. Computation procedure and algorithm pseudo code

The flowchart in Figure 4 shows the data processing steps and algorithm components of our localized contour tree method. The data processing steps include: (1) smooth the DEM with a Gaussian or median filter; (2) generate contours from the smoothed DEM by choosing the elevation of the base contour and the contour interval; (3) identify seed contours and construct local contour tree based on the topological relationship between the concentric closed contours; (4) search and identify all quasi-pour contours and simplify the local contour tree to the depression tree; (5) determine true pour contours and its spill elevation based on quasi-pour contour using an incremental expansion algorithm; and (6) calculate planimetric, volumetric, and shape properties for each surface depression defined by the true pour contour. Algorithm pseudo codes for key technical components are given in Table 1. Algorithms and mathematical equations used for computing planimetric, volumetric, and shape properties can be found in Liu and Wang (2008) and Liu *et al.* (2010).

The algorithm has been implemented using Microsoft Visual C++ .NET programming language and ArcObjects SDK for .NET. An array is declared as CONTOUR, which stores the information for each closed contour. The member variables of the array CONTOUR include the contour unique identification number (UIN), contour elevation (CE), sink point elevation (SPE), inwards adjacent contour neighbors (NBR), outwards adjacent contour unique identification number (OUIN), outwards adjacent contour elevation (OCE), and depression level (DL). If no outwards adjacent contour exists, the OUIN and OCE are set as −1. To derive the NBR for each contour, we used the ArcGIS 'Polygon Neighbors' geoprocessing tool. The contour line feature layer was first converted to non-overlapping polygon feature layer and then used as the input for the 'Polygon Neighbors' tool, which finds the neighbors of each contour polygon and records

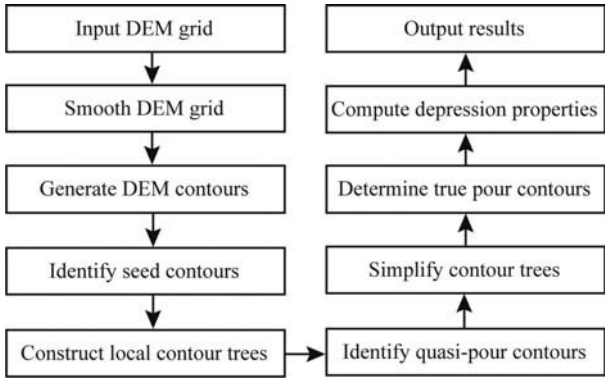

Figure 4. Flowchart in our localized contour tree method.

Table 1. (a) Pseudo-code for identifying all quasi-pour contours and assigning level number to each depression; (*b*) pseudo-code for determining true pour contours based on quasi contours with an incremental expansion algorithm.

(*a*)

```
Function IdentifyQuasiPourContour
  LBQ ← SEED
  level ← 1
  condition ← true
  While condition
    While LBQ is not empty
      s ← LBQ.top()
      LBQ.pop(s)
      While s.OUIN ≠ -1 and s.CE < s.OCE
        t ← CONTOUR[s.OUIN]
        If t.NBR = 1 Then
          s ← t
        End If
      End While
      UBQ.push(s)
    End While
    If UBQ.size > 0 Then
      QPOUR.add(level, UBQ)
      level ← level + 1
      While UBQ is not empty
        s ← UBQ.top()
        UBQ.pop(s)
        If s.OUIN ≠ -1 and s.CE < s.OCE
          t ← CONTOUR[s.OUIN]
          If t.NBR > 1 and FLAG[t] = false
            LBQ.push(t)
            FLAG[t] ← true
    Else
      condition ← false
    End If
  End While
End Function
```

(*b*)

```
Function IdentifyTruePourContour
  D = contour interval
  W = contour elevation difference
  For level =1 to max(level)
    LBQ ← QPOUR[level]
    For each quasi pour contour (s) in
      LBQ
      low ← s.CE
      high ← s.CE + D
      While (high - low < W)
        mid ← (low + high) / 2
        If contour(mid) is closed and only
          encloses contour(s) Then
          low ← mid
        Else If contour(mid) is open
          high ← mid
        End If
      End While
      If contour(high) is closed contour
        Then
        UBQ.push(high)
      Else If contour(mid) is closed contour
        Then
        UBQ.push(mid)
      Else If contour(low) is closed contour
        Then
        UBQ.push(low)
      End If
    End For
    TPOUR.add(level, UBQ)
  End For
End Function
```

the statistics in the output table. A priority queue is declared as SEED, which has the same member variables as CONTOUR. We prioritize the local contour tree construction in terms of the elevation value of the identified seed contours, and the seed contour with the lowest CE has the top priority and is first processed in the queue. The member functions of the priority queue include SEED.push(), SEED.top(), and SEED.pop(), which respectively support the operations of inserting a contour node into the queue, searching the lowest elevation contour node from the queue, and deleting the lowest elevation contour node from the queue. By looping through the array CONTOUR, the contours with no NBR (NBR = 0) are determined as seed contours and inserted into the priority queue SEED through the member function SEED.push(). Another two priority queues are declared as LBQ and UBQ, which store the contour nodes representing the lower and upper bound at each depression level, respectively. The array FLAG marks the contour nodes that have been processed and pushed into the queue. Two maps are declared as QPOUR and TPOUR, which store the set of quasi-pour contours and true pour contours at

each depression level, respectively. Maps are associative containers that store elements formed by key/value pairs and are accessible by key and by index.

4. Application results

We applied our new method to a case study area in Crow Wing County, Minnesota (Figure 5). The rectangular case study area is 3 km long in west–east direction and 2.4 km wide in south–north direction with a total area of 7.2 km^2. The surface elevation ranges from 373 m to 425 m. It is part of a glaciated plain of the Prairie Pothole Region of North America. There are numerous small surface depressions created by the retreating glaciers. Many of these glaciated surface depressions are covered by pooled water seasonally or permanently, forming a wetland ecosystem and landscape. The LiDAR data for Crow Wing County were acquired on 9 May 2007 (MINNESOTA GEOSPATIAL INFORMATION OFFICE 2008), which is freely available from Minnesota Geospatial Information Office (ftp://ftp.lmic.state.mn.us/pub/data/elevation/lidar/county/crowwing/. Accessed September 2014). The bare-earth LiDAR DEM is in the map projection of Universal Transverse Mercator (UTM) Zone 15N and referenced to horizontal datum-NAD83 and vertical datum NAVD88. The LiDAR DEM has 1 m spatial resolution and its root mean squared error (RMSE) of vertical measurements was estimated to be 28.95 cm based on 118 GPS check points (MERRICK & COMPANY 2008). An edge-preserving filter, 3 × 3 median filter, was used to smooth the LiDAR DEM. The shaded relief map of the bare-earth LiDAR DEM is shown in Figure 6.

Based on the smoothed bare-earth LiDAR DEM, we generated the vector contour representation by setting the base contour to be 370 m and the contour interval to be 0.5 m. The localized contour tree method was then applied to the contours to identify surface depressions. Figure 7 shows the detected surface depressions and their levels. In total, 267 disjoined surface depressions are detected, in which 244 are single-level simple depressions and 23 are multilevel complex surface depressions. For each disjoined surface depression, their geometric and topological properties have been computed. Table 2 shows

Figure 5. A case study area in Crow Wing County, Minnesota.

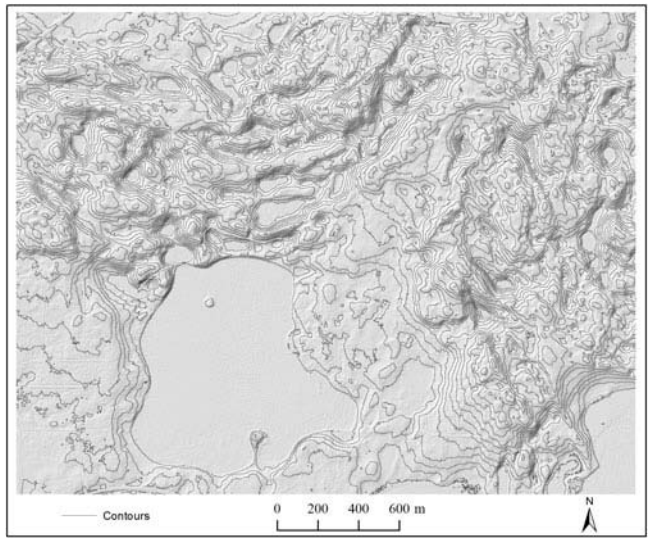

Figure 6. Shaded relief map with contours for the study area.

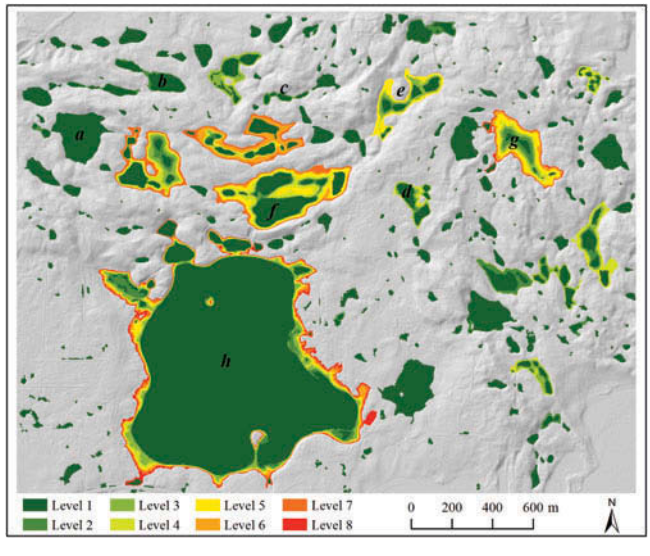

Figure 7. Localized contour tree depression analysis result for the study area.

the geometric and topological properties of a number of selected surface depressions: ***a, b, c, d, e, f, g,*** and ***h*** (Figure 7). The summary statistics of all the detected surface depressions for the case study area are shown in Table 3.

The surface depressions detected from our local contour tree method are compared to those from the Whitebox stochastic depression analysis tool. The stochastic depression analysis was conducted on the LiDAR DEM grid with 100 iterations. The probability of being part of a surface depression was calculated for each grid cell. Those grid cells with a probability value not lower than 0.7 were considered as real depression cells. Such cells

Table 2. Geometric and topological properties of selected depressions.

Depression	*a*	*b*	*c*	*d*	*e*	*f*	*g*	*h*
Centroid (lat, lon)	(46.507, −93.924)	(46.510, −93.919)	(46.509, −93.911)	(46.504, −93.902)	(46.509, −93.903)	(46.505, −93.911)	(46.507, −93.896)	(46.497, −93.914)
Spill elevation (m)	396.0	386.5	392.5	405.5	399.0	393.0	405.0	384.5
Surface area (m^2)	45,814	20,883	6,536	22,749	43,049	123,690	62,989	998,027
Max depth (m)	16.86	7.72	5.81	5.11	10.60	12.90	19.28	5.57
Mean depth (m)	7.08	3.57	1.77	1.58	3.83	7.00	5.91	4.38
Volume (m^3)	324,706	74,601	11,532	36,017	165,089	865,991	372,480	4,366,404
Compactness	0.35	0.21	0.16	0.28	0.14	0.31	0.18	0.13
Circularity	0.82	0.49	0.35	0.67	0.35	0.81	0.54	0.76
Asymmetry	0.05	0.77	0.80	0.34	0.59	0.59	0.52	0.12
Complexity level	1	2	3	4	5	6	7	8

Table 3. Summary statistics of depressions.

	Surface area (m^2)	Perimeter (m)	Max depth (m)	Mean depth (m)	Storage volume (m^3)
Minimum	51	40	0.16	0.05	3
Maximum	998,027	8218	19.28	7.08	4,366,404
Mean	7521	239	2.08	0.83	31,330
Median	515	113	0.79	0.31	155
Sum	2,008,230	63,694	NA	NA	8,365,218

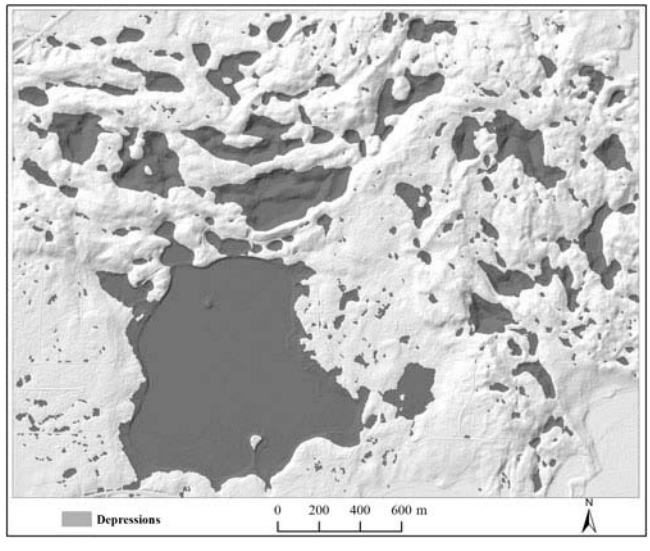

Figure 8. Whitebox stochastic depression analysis result for the study area.

were detected as depression cells 70 or more times out of 100 iterations. Subsequently, the morphology operator was applied to the detected depression cells to remove small erroneous holes and to smooth the boundaries of depressions. Figure 8 shows the depression features detected by the Whitebox stochastic depression analysis tool. There were 310 disjoined depressions identified with the Whitebox tool. The surface area of these depressions ranged from 101 m^2 to 992,113 m^2, with a median size of 401 m^2. The total surface area of all depressions was 2,021,727 m^2, which was larger than that detected by our method by 0.6%. This is because some shallow surface depressions were not captured and represented by the contour lines with a contour interval of 0.5 m. The Whitebox stochastic depression analysis tool does not have functions to derive geometric properties for individual surface depressions, let alone the nested hierarchical relationships among depressions inside a large complex depression like ***e*** shown in Figure 2b. In terms of running time, the Whitebox stochastic depression analysis took approximately 5 hours for the study area, with an average speed of 3 minutes per iteration on a computer with a 3.40-GHz i7-3770 CPU and 12 GB of RAM. In contrast, our localized contour tree method took approximately 6 minutes, which was 50 times faster than the Whitebox method.

5. Discussion

Our localized contour tree method is fundamentally different from the previous raster-based methods for surface depression detection. The rationale used in our method for surface depression detection is the same as the reasoning process that a human interpreter visually identifies surface depressions from a vector-based contour map. The design of our method is based on a core concept 'pour contour' that we introduce for the first time in surface depression studies. The graph theory-based algorithms have been introduced to implement different technical components of our method. In our method, we treat the surface depression detection problem as the identification of a set of concentric contours with an increasing elevation outward, which is represented by a contour tree. The delineation of surface depressions in our method is realized by identifying and refining pour contours. The search for surface depressions only occurs locally surrounding the seed contours rather than globally over all contours for the entire study area. The breath-first priority search is used to construct and grow local contour trees, identify quasi-pour contours, and simplify the contour tree. Localized contour tree construction and optimized graph theory-based search algorithms make our method computationally efficient and fast. The detection results for surface depression are reliable and consistent with human interpretation results.

Our method detects and represents each disjoined surface depression as one local contour tree. A disjointed surface depression is spatially independent of other surface depressions. When fully flooded, water in a disjointed surface depression will spill out and become overland flow, rather than directly merging with other surface depressions. A disjoined surface depression can be a single depression represented by a single-branch contour tree or a complex nested depression represented by a multibranch contour tree. All disjointed surface depressions in the study area correspond to a forest of many local contour trees.

Our method explicitly derives the geometric and topological properties of surface depressions. This has gone beyond the previous raster-based methods, which focused on surface depression detection and filling without much attention to quantification of surface depressions. By precisely determining the position of true pour contours as the boundaries of surface depressions, our method is able to accurately compute planimetric, volumetric, and shape properties for each individual surface depression. The depression tree simplified from contour tree explicitly describes the nested hierarchical structure of a complex depression, the level of composite depression, and the overall complexity of a disjoined depression quantitatively. The numerical information about semantic properties and structures of surface depressions derived from our method is valuable for many applications, such as simulating and modeling surface runoff and peak stream flows over time in hydrological analysis, determining local and regional water storage capability, estimating water evaporation and infiltration loss, and predicting water volume changes in limnological and wetland studies, etc.

The reliability and accuracy of the surface depressions detected by our method may be influenced by a number of factors. The spatial resolution and vertical accuracy of the original topographical data largely determine the minimum depression size and depth that we can reliably detect and delineate. The detection of smaller and shallower surface depressions demands higher spatial resolution and vertical accuracy of topographic data. The original LiDAR DEM data used in our application example has 1 m spatial resolution and a vertical accuracy of 28 cm (RMSE). It should be able to resolve a 2 m or larger surface depression with a depth of over 50 cm according to the Shannon sampling

theorem. Since our method is based on the vector-based contour representation, the option of the base contour line and particularly the contour interval would also influence the depression detection result. The selection of a large contour interval will generate few contour lines and increase computation speed of our method, but some shallow surface depressions would be missed during the contouring process. A small contour interval will help to detect shallow depressions, but results in an increased computation. It should be noted that the computed geometric and topological properties of the detected surface depressions in our method are accurate and are not influenced by the selection of the contour interval because an incremental expansion algorithm component is included to find the true pour contour. When the contour interval is sufficiently small, the quasi-pour contours would be very close to true pour contours, and the incremental expansion of quasi-contours may become unnecessary. The horizontal location difference between a quasi-pour contour and its true pour contour in gentle and flat terrain would be much larger than that in a steep terrain. As a general guideline, the target minimum size of surface depression to be mapped should be at least two or three times larger than spatial resolution of original topographical data, and the target minimum depth of surface depressions to be mapped should be larger than the contour interval as well as the vertical accuracy of original topographical data.

As in previous raster-based methods, the detected surface depressions could be real surface depressions or artifact depressions due to data noise and data processing errors. Since most artifact surface depressions are small, shallow, and irregular in shapes, smoothing the original topographical data prior to contouring can help reduce artifact depressions in our method. In addition, after we derive geometric properties for all surface depressions, we can choose appropriate threshold values for surface area, depth, and shape index to find those small, shallow, and irregular digital depressions to be removed as artifacts. Further treatment of artifact depressions is beyond the scope of the present work, and the reader is referred to Lindsay and Creed (2006) for a review of methods for artifact depression discrimination.

It should be noted that the reliability of the geometric properties of surface depressions, particularly depth and storage volume, is subject to the season of topographical data acquisitions. For instance, LiDAR remote sensing generally cannot penetrate water and thick vegetation. LiDAR data acquired during dry and leaf-off conditions on the ground are preferred for depression analysis. Even during the dry season some surface depressions may be partially covered by water, such as the Agate Lake shown in Figure 5. In this case, the derived depth and storage volume of the corresponding depressions would be significantly underestimated. The estimated volumetric properties need to be corrected by incorporating other sources of information or simply using the empirical statistical relationship between volume and surface area (Gleason *et al.* 2007).

6. Conclusions

Surface depressions are abundant in topographically complex landscapes, and they exert significant influences on hydrological, ecological, and biogeochemical processes at local and regional scales. The recent emergence of LiDAR and InSAR remote sensing technologies provides an extraordinary capability for acquiring high-resolution topographical data, which makes it possible to detect and quantify small surface depressions. In this research, we presented a new localized contour tree method that is able to fully exploit high-resolution topographic data for detecting, delineating, and characterizing surface depressions across scales with a multitude of geometric and topological properties.

Our localized contour tree method is developed by imitating human reasoning processes for interpreting and recognizing surface depressions from a vector-based contour map. In this research, we introduce a new concept of 'pour contour' and a graph theory-based contour tree representation for the first time to tackle the surface depression detection and delineation problem. The pour contour and the contour tree constitute the cornerstones of our new method, which is conceptually different from the previous raster-based depression detection methods. The localized growing and construction of contour trees and optimal tree search algorithms ensure the computational feasibility and efficiency of our method. The true pour contours determined from the incremental expansion of quasi-pour contours provide a solid foundation for accurately computing the various geometric properties of individual surface depressions. The depression tree simplified from the local contour tree provides a compact representation of the nested topological structure of complex surface depressions. The combination of planimetric, volumetric, and shape properties and the nested hierarchical structures derived from our method provides comprehensive and essential information for various environmental applications, such as fine-scale ecohydrological modeling, limnological analyses, and wetland studies. Our application example demonstrated that our localized contour tree method is functionally effective and computationally efficient.

Acknowledgment

The authors thank R.A. (Bob) MacMillan and two anonymous reviewers for their thoughtful comments.

References

Antonić, O., Hatic, D., and Pernar, R., 2001. DEM-based depth in sink as an environmental estimator. *Ecological Modelling*, 138 (1–3), 247–254. doi:10.1016/S0304-3800(00)00405-1

Arnold, N., 2010. A new approach for dealing with depressions in digital elevation models when calculating flow accumulation values. *Progress in Physical Geography*, 34 (6), 781–809. doi:10.1177/0309133310384542

Barnes, R., Lehman, C., and Mulla, D., 2014. Priority-flood: an optimal depression-filling and watershed-labeling algorithm for digital elevation models. *Computers & Geosciences*, 62 (0), 117–127. doi:10.1016/j.cageo.2013.04.024

Boyell, R.L. and Ruston, H., 1963. Hybrid techniques for real-time radar simulation. *Proceedings of the fall joint computer conference*, 12–14 November. Piscataway, NJ: IEEE, 445–458.

Chu, X., *et al.*, 2013. Dynamic puddle delineation and modeling of puddle-to-puddle filling-spilling-merging-splitting overland flow processes. *Water Resources Research*, 49 (6), 3825–3829. doi:10.1002/wrcr.v49.6

Dunne, T., Zhang, W., and Aubry, B.F., 1991. Effects of rainfall, vegetation, and microtopography on infiltration and runoff. *Water Resources Research*, 27 (9), 2271–2285. doi:10.1029/91WR01585

Finkl, C.W., Benedet, L., and Andrews, J.L., 2005. Interpretation of seabed geomorphology based on spatial analysis of high-density airborne laser bathymetry. *Journal of Coastal Research*, 213 (3), 501–514. doi:10.2112/05-756A.1

Frei, S., Lischeid, G., and Fleckenstein, J., 2010. Effects of micro-topography on surface–subsurface exchange and runoff generation in a virtual riparian wetland—A modeling study. *Advances in Water Resources*, 33 (11), 1388–1401. doi:10.1016/j.advwatres.2010.07.006

Gleason, R.A., *et al*., 2007. *Estimating water storage capacity of existing and potentially restorable wetland depressions in a subbasin of the Red River of the North* [online]. U.S. Geological Survey Open-File Report 2007-1159, 35 p. Available from: http://pubs.usgs.gov/of/2007/1159/

Guo, J.C.Y., 1999. Detention storage volume for small urban catchments. *Journal of Water Resources Planning and Management*, 125 (6), 380–382. doi:10.1061/(ASCE)0733-9496(1999)125:6(380)

Hayashi, M. and Van Der Kamp, G., 2000. Simple equations to represent the volume–area–depth relations of shallow wetlands in small topographic depressions. *Journal of Hydrology*, 237 (1–2), 74–85. doi:10.1016/S0022-1694(00)00300-0

Hayashi, M., Van Der Kamp, G., and Schmidt, R., 2003. Focused infiltration of snowmelt water in partially frozen soil under small depressions. *Journal of Hydrology*, 270 (3–4), 214–229. doi:10.1016/S0022-1694(02)00287-1

Huang, W., Deng, C., and Day, M.J., 2014. Differentiating tower karst (fenglin) and cockpit karst (fengcong) using DEM contour, slope, and centroid. *Environmental Earth Sciences*, 72 (2), 407–416.

Hubbard, D.E. and Linder, R.L., 1986. Spring runoff retention in prairie pothole wetlands. *Journal of Soil & Water Conservation*, 41 (2), 122–125.

Jenson, S. and Domingue, J., 1988. Extracting topographic structure from digital elevation data for geographic information system analysis. *Photogrammetric Engineering and Remote Sensing*, 54 (11), 1593–1600.

Kweon, I.S. and Kanade, T., 1994. Extracting topographic terrain features from elevation maps. *CVGIP: Image Understanding*, 59 (2), 171–182. doi:10.1006/ciun.1994.1011

Lefsky, M.A., *et al*., 2002. Lidar remote sensing for ecosystem studies. *BioScience*, 52 (1), 19–30.

Li, S., *et al.*, 2011. Lidar DEM error analyses and topographic depression identification in a hummocky landscape in the prairie region of Canada. *Geomorphology*, 129 (3–4), 263–275. doi:10.1016/j.geomorph.2011.02.020

Lindsay, J.B., 2004. *Coping with topographic depression in digital terrain analysis*. Thesis (PhD). University of Western Ontario.

Lindsay, J.B., 2005. The terrain analysis system: a tool for hydro-geomorphic applications. *Hydrological Processes*, 19 (5), 1123–1130. doi:10.1002/(ISSN)1099-1085

Lindsay, J.B., 2014. The whitebox geospatial analysis tools project and open-access GIS. *Proceedings of the GIS research UK 22nd annual conference*, 16–18 April. Bath: The University of Glasgow.

Lindsay, J.B. and Creed, I.F., 2005. Removal of artifact depressions from digital elevation models: towards a minimum impact approach. *Hydrological Processes*, 19 (16), 3113–3126. doi:10.1002/(ISSN)1099-1085

Lindsay, J.B. and Creed, I.F., 2006. Distinguishing actual and artefact depressions in digital elevation data. *Computers & Geosciences*, 32 (8), 1192–1204. doi:10.1016/j.cageo.2005.11.002

Lindsay, J.B. and Seibert, J., 2013. Measuring the significance of a divide to local drainage patterns. *International Journal of Geographical Information Science*, 27 (7), 1453–1468. doi:10.1080/13658816.2012.705289

Liu, H. and Wang, L., 2008. Mapping detention basins and deriving their spatial attributes from airborne LiDAR data for hydrological applications. *Hydrological Processes*, 22 (13), 2358–2369. doi:10.1002/(ISSN)1099-1085

Liu, H., *et al.*, 2010. An object-based conceptual framework and computational method for representing and analyzing coastal morphological changes. *International Journal of Geographical Information Science*, 24 (7), 1015–1041. doi:10.1080/13658810903270569

Loos, M. and Elsenbeer, H., 2011. Topographic controls on overland flow generation in a forest–An ensemble tree approach. *Journal of Hydrology*, 409 (1–2), 94–103. doi:10.1016/j.jhydrol.2011.08.002

Macmillan, R., *et al*., 1993. Using hydrological models and geographic information systems to assist with the management of surface water in agricultural landscapes. *In*: R. Haines-Young, ed. *Landscape ecology and geographic information systems*. Boca Raton, FL: CRC Press, 181–209.

Maidment, D.R., 2002. *Arc Hydro: GIS for water resources*. Redlands, CA: ESRI Press.

Mark, D.M., 1988. Network models in geomorphology. *In*: *Modelling geomorphological systems*. Hoboken, NJ: Wiley, 73–97.

Marks, D., Dozier, J., and Frew, J., 1984. Automated basin delineation from digital elevation data. *Geo-processing*, 2 (3), 299–311.

Martz, L.W. and Garbrecht, J., 1999. An outlet breaching algorithm for the treatment of closed depressions in a raster DEM. *Computers & Geosciences*, 25 (7), 835–844. doi:10.1016/S0098-3004(99)00018-7

Martz, L.W. and Jong, E.D., 1988. CATCH: a FORTRAN program for measuring catchment area from digital elevation models. *Computers & Geosciences*, 14 (5), 627–640. doi:10.1016/0098-3004(88)90018-0

Mcgrath, G.S., Paik, K., and Hinz, C., 2012. Microtopography alters self-organized vegetation patterns in water-limited ecosystems. *Journal of Geophysical Research: Biogeosciences (2005–2012)*, 117 (G3), G03021. doi:10.1029/2011JG001870

Merrick & Company, 2008. *Map accuracy report, countywide imagery & DEM, crow wing county* [online]. Available from: http://www.dot.state.mn.us/surveying/pdf/mapaccreports/Map%20Accuracy%20Report%20Crow%20Wing.pdf [Accessed September 2014].

Minnesota Geospatial Information Office, 2008. *LiDAR elevation, Crow Wing County, Minnesota, 2008*. [online]. Available from: http://www.mngeo.state.mn.us/chouse/metadata/lidar_crowwing2008.html [Accessed 1 November 2014].

Moser, K., Ahn, C., and Noe, G., 2007. Characterization of microtopography and its influence on vegetation patterns in created wetlands. *Wetlands*, 27 (4), 1081–1097. doi:10.1672/0277-5212(2007)27[1081:COMAII]2.0.CO;2

Muehrcke, P.C., Muehrcke, J.O., and Kimerling, A., 1992. *Map use: reading. Analysis and Interpretation*. 3rd ed. Madison, WI: JP Publications.

O'Callaghan, J.F. and Mark, D.M., 1984. The extraction of drainage networks from digital elevation data. *Computer Vision, Graphics, and Image Processing*, 28 (3), 323–344. doi:10.1016/S0734-189X(84)80011-0

Planchon, O. and Darboux, F., 2002. A fast, simple and versatile algorithm to fill the depressions of digital elevation models. *Catena*, 46 (2–3), 159–176. doi:10.1016/S0341-8162(01)00164-3

Rosenberry, D.O. and Winter, T.C., 1997. Dynamics of water-table fluctuations in an upland between two prairie-pothole wetlands in North Dakota. *Journal of Hydrology*, 191 (1–4), 266–289. doi:10.1016/S0022-1694(96)03050-8

Scanlon, T.M., *et al.*, 2007. Positive feedbacks promote power-law clustering of Kalahari vegetation. *Nature*, 449 (7159), 209–212. doi:10.1038/nature06060

Schwarz, B., 2010. LIDAR: mapping the world in 3D. *Nature Photonics*, 4 (7), 429–430. doi:10.1038/nphoton.2010.148

Sedgewick, R., 1998. Chapter 5. Recursion and trees. *In*: *Algorithms in C++, Parts 1–4: fundamentals, data structure, sorting, searching*. 3rd ed. Indianapolis, IN: Pearson Education.

Simmons, M.E., Ben Wu, X., and Whisenant, S.G., 2011. Plant and soil responses to created microtopography and soil treatments in bottomland hardwood forest restoration. *Restoration Ecology*, 19 (1), 136–146. doi:10.1111/rec.2011.19.issue-1

Tarboton, D.G., Bras, R.L., and Rodriguez-Iturbe, I., 1991. On the extraction of channel networks from digital elevation data. *Hydrological Processes*, 5 (1), 81–100. doi:10.1002/(ISSN)1099-1085

Thompson, S.E., Katul, G.G., and Porporato, A., 2010. Role of microtopography in rainfall-runoff partitioning: an analysis using idealized geometry. *Water Resources Research*, 46 (7). doi:10.1029/2009WR008835

Tribe, A., 1992. Automated recognition of valley lines and drainage networks from grid digital elevation models: a review and a new method. *Journal of Hydrology*, 139 (1–4), 263–293. doi:10.1016/0022-1694(92)90206-B

Ussyshkin, V. and Theriault, L., 2011. Airborne LiDAR: advances in discrete return technology for 3D vegetation mapping. *Remote Sensing*, 3 (12), 416–434. doi:10.3390/rs3030416

Wang, L. and Liu, H., 2006. An efficient method for identifying and filling surface depressions in digital elevation models for hydrologic analysis and modelling. *International Journal of Geographical Information Science*, 20 (2), 193–213. doi:10.1080/13658810500433453

White, S.A. and Wang, Y., 2003. Utilizing DEMs derived from LIDAR data to analyze morphologic change in the North Carolina coastline. *Remote Sensing of Environment*, 85 (1), 39–47. doi:10.1016/S0034-4257(02)00185-2

Wörman, A. and Kronnäs, V., 2005. Effect of pond shape and vegetation heterogeneity on flow and treatment performance of constructed wetlands. *Journal of Hydrology*, 301 (1–4), 123–138. doi:10.1016/j.jhydrol.2004.06.038

Wu, Q., Lane, C., and Liu, H., 2014. An effective method for detecting potential woodland vernal pools using high-resolution LiDAR data and aerial imagery. *Remote Sensing*, 6 (11), 11444–11467. doi:10.3390/rs61111444

Yu, W.-B., *et al.*, 2014. An efficient algorithm for depression filling and flat-surface processing in raster DEMs. *IEEE Geoscience and Remote Sensing Letters*, 11 (12), 2198–2202. doi:10.1109/LGRS.2014.2324616